Original Article

MOLECULAR METABOLISM

# URAT1-selective inhibition ameliorates insulin resistance by attenuating diet-induced hepatic steatosis and brown adipose tissue whitening in mice

**Yoshiro Tanaka, Tomohisa Nagoshi*, Hirotake Takahashi, Yuhei Oi, Akira Yoshii, Haruka Kimura, Keiichi Ito, Yusuke Kashiwagi, Toshikazu D. Tanaka, Michihiro Yoshimura**

## ABSTRACT

**Objective:** Accumulating evidence indicates that high uric acid (UA) is strongly associated with obesity and metabolic syndrome and drives the development of nonalcoholic fatty liver disease (NAFLD) and insulin resistance. Although urate transporter-1 (URAT1), which is primarily expressed in the kidneys, plays a critical role in the development of hyperuricemia, its pathophysiological implication in NAFLD and insulin resistance remains unclear. We herein investigated the role and functional significance of URAT1 in diet-induced obese mice.

**Methods:** Mice fed a high-fat diet (HFD) for 16–18 weeks or a normal-fat diet (NFD) were treated with or without a novel oral URAT1-selective inhibitor (dotinurad [50 mg/kg/day]) for another 4 weeks.

**Results:** We found that URAT1 was also expressed in the liver and brown adipose tissue (BAT) other than the kidneys. Dotinurad administration significantly ameliorated HFD-induced obesity and insulin resistance. HFD markedly induced NAFLD, which was characterized by severe hepatic steatosis as well as the elevation of serum ALT activity and tissue inflammatory cytokine genes (chemokine ligand 2 (Ccl2) and tissue necrosis factor $\alpha$ (TNF$\alpha$)), all of which were attenuated by dotinurad. Similarly, HFD significantly increased URAT1 expression in BAT, resulting in lipid accumulation (whitening of BAT), and increased the production of tissue reactive oxygen species (ROS), which were reduced by dotinurad via UCP1 activation.

**Conclusions:** In conclusion, a novel URAT1-selective inhibitor, dotinurad, ameliorates insulin resistance by attenuating hepatic steatosis and promoting rebrowning of lipid-rich BAT in HFD-induced obese mice. URAT1 serves as a key regulator of the pathophysiology of metabolic syndrome and may be a new therapeutic target for insulin-resistant individuals, particularly those with concomitant NAFLD.



**Keywords** Uric acid; URAT1; Insulin resistance; NAFLD; Metabolic syndrome

## 1. INTRODUCTION

Increasing evidence indicates that elevated serum uric acid (UA) levels are associated with several cardiovascular diseases, chronic kidney disease, and nonalcoholic fatty liver disease (NAFLD) [1–3]. Patients with hyperuricemia are also predisposed to metabolic syndrome, a pathological condition that involves insulin resistance, chronic inflammation, and the synthesis of reactive oxygen species (ROS) [4,5]. Although previous studies showed that hyperuricemia itself leads to these pathological conditions in various tissues [4,6], the precise mechanism by which high UA induces insulin resistance has not been fully understood.

Urate transporter-1 (URAT1) is a UA reabsorption system and is primarily expressed in the epithelial cells of proximal tubules in the renal cortex [7,8]. The expression of URAT1 in the kidneys is upregulated under hyperuricemic and hyperinsulinemic conditions such as metabolic syndrome [9]. The increased uptake of UA in adipocytes induces inflammation and the synthesis of ROS [1], which contributes to systemic insulin resistance. Furthermore, benzbromarone, a nonselective URAT1 inhibitor, improved systemic insulin resistance in patients with

Division of Cardiology, Department of Internal Medicine, The Jikei University School of Medicine, 3-25-8, Nishi-Shimbashi, Minato-ku, Tokyo, 105-8461, Japan

*Corresponding author. Fax: +81 3 3459 6043.

E-mails: tanakayoshiro@jikei.ac.jp (Y. Tanaka), tnagoshi@jikei.ac.jp (T. Nagoshi), h.takahashi@jikei.ac.jp (H. Takahashi), yoi@jikei.ac.jp (Y. Oi), a.yoshii@jikei.ac.jp (A. Yoshii), kimuraha@jikei.ac.jp (H. Kimura), keke_ito@yahoo.co.jp (K. Ito), y-kashiwa@jikei.ac.jp (Y. Kashiwagi), tanakatd@jikei.ac.jp (T.D. Tanaka), m.yoshimura@jikei.ac.jp (M. Yoshimura).

*Abbreviations:* AUC, area under the curve; BAT, brown adipose tissue; Ccl2, chemokine ligand 2; Doti, dotinurad; eWAT, epididymal white adipose tissue; HFD, high-fat diet; IPGTT, intraperitoneal glucose tolerance test; ITT, insulin tolerance test; iWAT, inguinal white adipose tissue; MDA, malondialdehyde; NAFLD, nonalcoholic fatty liver disease; NFD, normal-fat diet; ROS, reactive oxygen species; TNF$\alpha$, tissue necrosis factor $\alpha$; UA, uric acid; UCP1, uncoupling protein 1; URAT1, urate transporter-1

Received October 4, 2021 • Revision received November 29, 2021 • Accepted November 29, 2021 • Available online 1 December 2021

https://doi.org/10.1016/j.molmet.2021.101411

 

chronic heart failure [10], indicating that URAT1 is closely related to the regulation of systemic insulin resistance.

NAFLD has become the most common chronic liver disease in metabolic syndrome and can progress to liver cirrhosis and hepatocellular carcinoma [11]. NAFLD ranges from plain steatosis to advanced nonalcoholic steatohepatitis (NASH) characterized by steatosis associated with inflammation and fibrosis [12]. Hyperuricemia also promotes the development of steatosis in *in vitro* [13] and *in vivo* models [4], and the enhanced UA uptake in human hepatoma HepG2 cells via URAT1 elicits an inflammatory response [14]. However, the role and functional significance of URAT1 in the pathophysiology of NAFLD has not been completely understood.

Adipose tissues are broadly classified into two categories: white adipose tissue (WAT) serves largely to store calories, and its inflammation is generally responsible for metabolic disorders, whereas brown adipose tissue (BAT) promotes energy utilization and generates heat using metabolic fuel via a BAT-specific protein, uncoupling protein 1 (UCP1) [15,16]. Diet-induced obesity leads to BAT "whitening", which is associated with the accumulation of large lipid droplets and mitochondrial dysfunction and loss, resulting in impaired glucose metabolism [15,17,18]. Diet-induced obesity also causes the dysfunction of WAT per se, leading to the impairment of glucose metabolism, and the activation of URAT1 has been reported to be involved in this pathophysiological mechanism [1,19]; however, the role and functional significance of URAT1 in BAT remains unknown.

Selective uric reabsorption inhibitors (SURIs), such as lesinurad, dotinurad, and verinurad, have been recently developed as potent uricosuric agents by selectively inhibiting URAT1 [20–22]. Among them, dotinurad is widely used in clinical practice in Japan for the treatment of patients with hyperuricemia [23]. To better understand the role and the functional significance of URAT1 in obesity-induced metabolic disorders, we investigated whether the URAT1-selective inhibitor treatment ameliorates systemic insulin resistance, NAFLD, and adipose tissue dysfunction using diet-induced obese mice.

## 2. MATERIAL AND METHODS

### 2.1. Animal models

All animal procedures conformed to the National Institutes of Health Guide for the Care and Use of Laboratory Animals and were approved by the Animal Research Committee at the Jikei University School of Medicine (2016-038C6). Male C57BL/6 mice at 8 weeks of age were fed either normal-fat diet (NFD) or high-fat diet (HFD) for 16–18 weeks as described previously [24]. Where indicated, mice fed NFD or HFD received the URAT1-selective inhibitor dotinurad (50 mg/kg/day, kindly provided by Fuji Yakuhin Co., Saitama, Japan) for 4 weeks by dietary intake (Figure 1A). As the dietary intake of NFD and HFD mice was different during the protocol (Figure 1D), the concentration of dotinurad mixed into the diet was adjusted accordingly in order to equalize the dosage of dotinurad between the NFD and HFD mice groups.

At four weeks after the initiation of the dotinurad treatment, the mice were heparinized (1000 IU/kg, intraperitoneally [i.p.]) and anesthetized (0.3 mg/kg of medetomidine, 4.0 mg/kg of midazolam, and 5.0 mg/kg of butorphanol, i.p.) in order to eliminate suffering. Then, the liver, epididymal WAT (eWAT), inguinal WAT (iWAT), BAT, and the kidneys were excised and washed in PBS (Fujifilm, Wako pure Chemical Corporation) at 4 °C. After washing, tissues were snap-frozen in liquid nitrogen and stored at −80 °C until further analysis.

### 2.2. Plasma UA measurement

The plasma UA level was measured at 4 weeks after the initiation of dotinurad treatment using a UA assay kit (Sigma) according to the manufacturer's protocol as described previously [3].

### 2.3. Serum triglyceride, non-esterified fatty acids, and insulin concentration measurements

The blood was drawn immediately after the heart excision and centrifuged (3000 g, 10 min, 4 °C). The serum (supernatant) was collected into new tubes and frozen at −20 °C prior to the measurement. Serum triglyceride (TG) and non-esterified fatty acids (NEFA) were measured at 4 weeks after the initiation of dotinurad treatment using LabAssay Triglyceride (#LABTR G-M1, Fujifilm Wako Pure Chemical Corporation, Tokyo, Japan) and LabAssay NEFA (#294-63601, Fujifilm Wako Pure Chemical Corporation, Tokyo, Japan), respectively, according to the manufacturer's protocol as described previously [18]. Serum insulin levels were measured using the mouse insulin ELISA kit (Shibayagi, Gunma, Japan) according to the manufacturer's protocol [25].

### 2.4. Blood pressure and heart rate measurement

We used a noninvasive computerized tail-cuff system to measure blood pressure in conscious mice 4 weeks after the initiation of treatment with dotinurad (BP-98A-L, Softron Co., Ltd., Tokyo, 6 Japan). The mice were held in a small mouse pocket on a warming pad thermostatically controlled at 37 °C. Systolic and diastolic pressure and heart rate were calculated at three different times and averaged [18].

### 2.5. Glucose and insulin tolerance tests

Four weeks after the initiation of treatment with dotinurad, we performed a glucose tolerance test (IPGTT) and insulin tolerance tests (ITT), as described previously [18,24].

### 2.6. RNA isolation, reverse transcription, and real-time polymerase chain reaction

Polymerase chain reaction (PCR) for tissues was performed as described previously [24] using the primers for URAT1 (Applied Biosystems, Mm01236822_m1), UCP1 (Applied Biosystems, Mm01244861_m1), PGC1α (Applied Biosystems, Mm01208835_m1), Dio2 (Applied Biosystems, Mm00515664_m1), chemokine ligand 2 (Ccl2) (Applied Biosystems, Mm00441242_m1), tissue necrosis factor α (TNFα) (Applied Biosystems, Mm00443258_m1), and GAPDH (Applied Biosystems, Mn03302249_g1).

### 2.7. Immunoblotting

Immunoblotting was performed as described previously [24] with rabbit polyclonal anti-URAT1 (1:1500, 14937-1-AP; Proteintech, Tokyo, Japan), rabbit polyclonal anti-UCP1 (1:3000, U6382; Sigma–Aldrich, Tokyo, Japan), monoclonal mouse anti-β-actin (1:5000, A5316; Sigma–Aldrich, Tokyo, Japan), monoclonal rabbit anti-NLRP3 antibody (1:1000, #15101; Cell Signaling Technology, Tokyo, Japan), monoclonal rabbit anti-IL-1β antibody (1:500, #31202; Cell Signaling Technology, Tokyo, Japan), and anti-GAPDH (1:5000, #2118; Cell Signaling Technology, Tokyo, Japan). The signals were detected using chemiluminescence.

### 2.8. Histology and immune staining

The liver, eWAT, iWAT, and BAT were excised, washed in ice-cold PBS, and fixed with 10% formalin. The samples were embedded into paraffin, and 4 μm sections were prepared for histological analyses as

 

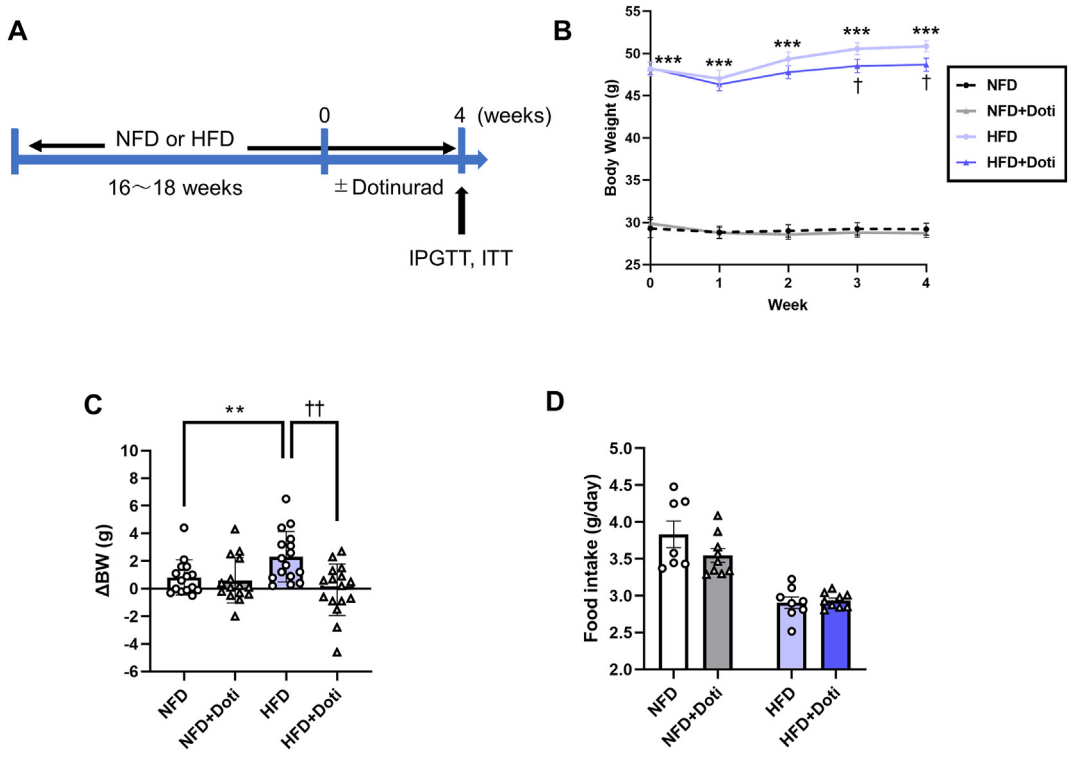


**Figure 1: Effects of URAT1-selective inhibitor treatment on body weight and plasma uric acid.** (A) A schematic diagram of the experimental protocol. (B) Body weight changes during the protocol (NFD, n = 10; NFD + Doti, n = 12; HFD, n = 13; HFD + Doti, n = 13). (C) The degree of body weight gain from baseline (NFD, n = 15; NFD + Doti, n = 15; HFD, n = 16; HFD + Doti, n = 16). (D) The dietary intake per day (NFD, n = 7; NFD + Doti, n = 9; HFD, n = 8; HFD + Doti, n = 9). Data are expressed as the mean ± SEM. (B) ***P < 0.001, **P < 0.01, and *P < 0.05 versus NFD at each time point; †P < 0.05 versus HFD at each time point. (C) **P < 0.01, NFD versus HFD; ††P < 0.01, HFD versus HFD + Doti. NFD, normal-fat diet; HFD, high-fat diet; Doti, dotinurad; IPGTT, intraperitoneal glucose tolerance test; ITT, insulin tolerance test.

described previously [18]. Hematoxylin and eosin-stained sections were visualized using ECLIPS 80i (Nikon Co., Tokyo, Japan). Adipocytes images in WAT were analyzed for adipocyte size using BZ-X800 analyzer software (Keyence Corp., Osaka, Japan) following the manufacturer's instructions [26]. The size of approximately 800–1000 adipocytes in WAT per mouse was assessed by measuring the diameter of the lipid droplets and averaged [27]. The area of about 100 lipid droplets and the size of about 200 brown adipocytes in BAT per mouse were measured in the image at 20× magnification using Image J software [28]. For immunohistochemical staining, fixed BAT sections were incubated with rabbit polyclonal anti-UCP1 antibody (1:500) (U6382; Sigma–Aldrich, Tokyo, Japan). The stained images were visualized and captured using ECLIPS 80i.

### 2.9. Serum alanine aminotransferase activity measurement

The blood was drawn immediately after the heart excision and centrifuged (3000 g, 10 min, 4 °C). The serum (supernatant) was collected into new tubes and frozen at −20 °C prior to serum alanine aminotransferase (ALT) activity measurement. ALT activity was measured using the ALT colorimetric assay kit (catalog #752, BioVision, Inc.) according to the manufacturer's protocol [29].

### 2.10. Pathology and staging of steatosis

Hematoxylin and eosin staining was performed for evaluating liver histology and grading liver injury using a scoring system for NASH established by Savari F et al. [12]. According to this standardized scoring system, the sum of steatosis (0–3), lobular inflammation (0–3), and hepatocellular ballooning degeneration (0–2) scores was considered to be the NAFLD activity score. The criteria were as follows: steatosis grade, 0: less than 5%; 1: between 5 and 33%; 2: between 33 and 66%; and 3: more than 66%. For lobular inflammation, minimal or absence of inflammatory cell accumulation (infiltration) was classified as grade 0, mild infiltration was classified as grade 1, moderate to severe infiltration was classified as grade 2, and severe inflammatory cell accumulation was classified as grade 3. Cell ballooning was classified as none (0), mild (few swollen cells; 1), and severe (many swollen cells; 2) based on its severity.

### 2.11. Liver malondialdehyde

Frozen liver tissue was homogenized in ice-cold RIPA buffer with protease inhibitor cocktail (Roche) and centrifuged (1,600 *g*, 10 min, 4 °C). The supernatant was used for the quantification of malondialdehyde (MDA) using the thiobarbituric acid reactive substance (TBARS) kit according to the manufacturer's protocols (Cayman Chemical, 700870). Briefly, the tissue lysates were allowed to react with thiobarbituric acid at 100 °C for 1 h, and the absorbance of the solution was measured at 530–540 nm [30]. The measurement values were corrected based on the protein concentration of the supernatant measured by the Bradford protein assay.

### 2.12. BAT ROS measurement

Frozen BAT was homogenized in cell lysis buffer (Cell Signaling Technology, Tokyo, Japan) with phenylmethylsulfonyl fluoride (PMSF) and centrifuged (14,000 *g*, 10 min, 4 °C). The tissue lysates were mixed with a dichlorofluorescein diacetate fluorescent (DCFH-DA) (Invitrogen, D399) probe (5 μM) for 1 h at 37 °C [31,32]. DCF

 

fluorescence was measured using a microplate reader (485 nm excitation and 527 nm emission) and corrected based on the protein concentration of the supernatant measured by the Bradford protein assay.

### 2.13. Primary brown adipocyte differentiation

Rat brown adipocytes derived from the interscapular BAT of adult SD rats were purchased from Cosmo Bio Co. and cultured using a Brown Adipocyte Culture Kit (PMC-BAT10-COS) according to the manufacturer's protocol. The cells were cultured for 7 days as described previously [16] and used in the following experimental protocols on day 8 after starvation in serum-free medium for 12 h.

### 2.14. Intracellular UA levels of primary brown adipocytes

The culture medium was pre-warmed for 30 min at 37 °C and UA (Sigma) was solubilized in the culture medium by vortexing. Then the mixture was heated for 30 min at 37 °C and passed through sterile 0.2 μm filters as described previously [33]. After 30 or 60 min of incubation with the indicated concentration of UA (0 mg/dl, 5 mg/dl, 15 mg/dl) with or without dotinurad (15 μM), each dish was washed twice with PBS and snap frozen. Brown adipocytes were collected and lysed in 100 μl cell lysis buffer (Cell Signaling Technology, Tokyo, Japan) with PMSF and centrifuged (13,000 *g*, 10 min, 4 °C). The UA levels in the supernatant were measured using a UA assay kit (Sigma) according to the manufacturer's protocol. Intracellular UA levels of primary brown adipocytes were corrected based on the protein concentration of the supernatant measured by the Bradford protein assay.

### 2.15. Statistical analysis

All quantitative data were presented as mean ± standard error of the mean (SEM) and analyzed using Prism 8 (GraphPad). For the comparison of two datasets, either the Mann—Whitney U test (non-normal distribution data) or the Student's t-test (normal distribution data) was performed. For multiple comparisons among ≥3 groups, one-way ANOVA with Tukey's method for post hoc comparisons and the non-parametric Kruskal—Wallis test with Dunn's multiple comparisons were performed. Two-sided P values $< 0.05$ were considered to indicate statistical significance.

## 3. RESULTS

### 3.1. Effects of URAT1-selective inhibitor treatment on body weight, plasma UA, and lipid profile in HFD-fed mice

The experimental protocol is shown in Figure 1A. After 16—18 weeks of HFD feeding, the mice developed considerable obesity, and treatment with dotinurad slightly but significantly reduced the body weight of HFD-fed mice at weeks 3 and 4 (Figure 1B and C). The weight loss in dotinurad-treated mice was not due to a decrease in dietary intake (Figure 1D). The plasma UA level in HFD-fed mice was significantly increased in comparison with that in NFD-fed mice, and dotinurad lowered it, although the differences failed to reach statistical significance (Table 1). The serum TG level in HFD-fed mice was increased in comparison with that in NFD-fed mice, and treatment with dotinurad significantly decreased it in both NFD- and HFD-fed mice (Table 1). Although dotinurad decreased the serum NEFA level in NFD-fed mice, no significant differences were observed between NFD- and HFD-fed mice with or without dotinurad treatment (Table 1). There were no significant between-group differences in blood pressure (Figure S1A) and heart rate (Figure S1B), indicating that the effects of dotinurad on the systemic sympathetic nerve activities are limited.

**Table 1** — Blood metabolic parameters of NFD- and HFD-fed mice treated with or without dotinurad in the fasting state.

| | NFD | NFD + Doti | HFD | HFD + Doti |
|---|---|---|---|---|
| UA (mg/dl) | 3.6 ± 0.2 | 3.3 ± 0.2 | 4.5 ± 0.2* | 4.0 ± 0.2 |
| TG (mg/dl) | 58 ± 2 | 30 ± 4*** | 77 ± 7* | 51 ± 2†† |
| NEFA (mEq/L) | 1.02 ± 0.06 | 0.58 ± 0.04*** | 1.07 ± 0.12 | 0.96 ± 0.03 |
| Glucose (mg/dl) | 139 ± 11 | 155 ± 22 | 264 ± 22*** | 209 ± 13 |
| Insulin (pg/ml) | *n.d.* | *n.d.* | 994 ± 101 | 561 ± 98†† |

NFD, Normal fat diet; Doti, dotinurad; HFD, high-fat diet; UA, uric acid; TG, triglyceride; NEFA, non-esterified fatty acids. [Uric acid] NFD, n = 5; NFD + Doti, n = 7; HFD, n = 6; HFD + Doti, n = 7; [TG] and [NEFA] NFD, n = 10; NFD + Doti, n = 6; HFD, n = 12; HFD + Doti, n = 7; [Glucose] NFD = 10; NFD + Doti = 6; HFD, n = 10; HFD + Doti, n = 8; [Insulin] HFD, n = 9; HFD + Doti, n = 8.
*n.d.* not detected.
Data are expressed as the mean ± SEM. ***P $< 0.001$ and *P $< 0.05$ versus NFD; ††P $< 0.01$, versus HFD.

### 3.2. URAT1-selective inhibitor treatment improves HFD-induced glucose intolerance and insulin resistance in HFD-fed mice

Previous reports showed that the expression of URAT1 in the kidney was upregulated in metabolic syndrome [9] and benzbromarone, a uricosuric agent, led to the improvement of systemic insulin resistance in patients with chronic heart failure [10]. Thus, we next examined the effects of URAT1-selective inhibitor treatment on glucose tolerance and insulin sensitivity. The fasting plasma glucose levels were increased in HFD mice, which tended to be lower in dotinurad-treated HFD-fed mice (HFD vs. HFD + Doti, P = 0.06) (Table 1). Similarly, dotinurad significantly decreased serum insulin concentrations in HFD mice under fasting conditions (Table 1). IPGTT and ITT demonstrated that HFD feeding induced glucose intolerance and insulin resistance, which were ameliorated by dotinurad treatment (Figure 2A and B). These results indicate that the selective inhibition of URAT1 significantly improves glucose tolerance and insulin sensitivity in HFD-induced obese mice.

### 3.3. The URAT1 expression levels in various tissues of NFD- and HFD-fed mice

To identify potential target cells of URAT1 in metabolic syndrome, we examined the URAT1 expression levels in various tissues. An abundant expression of URAT1 mRNA was observed in the kidneys, as expected (Figure 3A), whereas the expression levels in eWAT were the second highest after the kidneys. URAT1 mRNA was also detected at relatively low levels in the liver, iWAT, and BAT. The expression of URAT1 protein (but not mRNA) in the liver was decreased in HFD-fed mice in comparison with that in NFD-fed mice (Figure 3B and C). The URAT1 expression in eWAT was comparable between the groups (Figure 3B and D). In contrast, HFD increased the URAT1 expression in iWAT and even more dramatically in BAT (Figure 3B and E). In the kidneys, we found that the URAT1 protein expression (but not mRNA levels) tended to be higher in HFD-fed mice than in NFD-fed mice (P = 0.09) (Figure S2A and B), in line with the results of a previous study [9]. Dotinurad did not significantly affect the URAT1 expression in all tissues examined, regardless of the diet conditions (Figure 3B—E), although in the kidneys, the URAT1 expression was nonsignificantly higher in the NFD group treated with dotinurad via an unknown mechanism (Figures S2A and B).

 

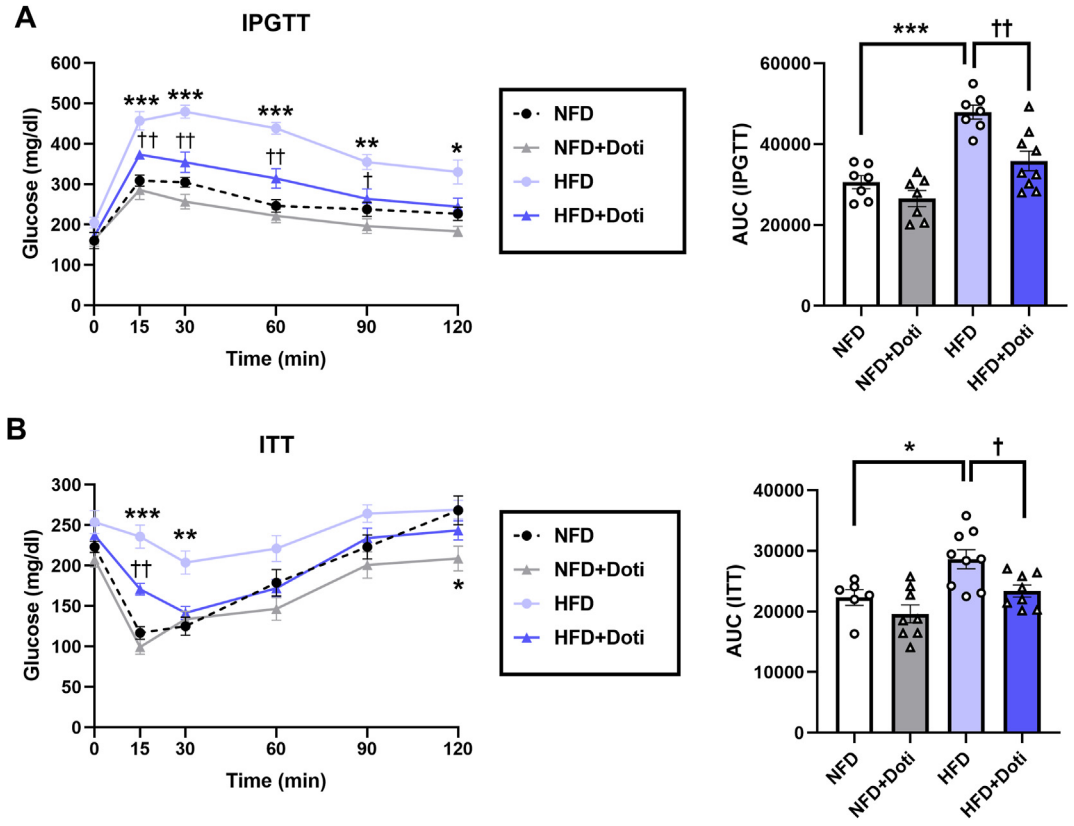


**Figure 2: Effects of URAT1-selective inhibitor treatment on HFD-induced insulin resistance.** (A) Plasma glucose levels during IPGTT and the area under the curve (AUC) (NFD, n = 7; NFD + Doti, n = 7; HFD, n = 7; HFD + Doti, n = 9). (B) Plasma glucose levels during ITT and the AUC (NFD, n = 6; NFD + Doti, n = 8; HFD, n = 9; HFD + Doti, n = 8). Data are expressed as the mean ± SEM. (Line graphs) ***P < 0.001, **P < 0.01, and *P < 0.05 versus NFD at each time point; ††P < 0.01 and †P < 0.05 versus HFD at each time point. (AUC) ***P < 0.001 and *P < 0.05, NFD versus HFD; ††P < 0.01 and †P < 0.05, HFD versus HFD + Doti.

### 3.4. URAT1-selective inhibitor treatment attenuates the development of HFD-induced NAFLD through the inhibition of inflammatory cytokines

We next examined whether URAT1-selective inhibitor treatment improves HFD-induced NAFLD in mice. Although dotinurad increased the liver weight in the NFD-fed group, it substantially attenuated HFD-induced hepatomegaly (Figure 4A and B). HFD feeding led to the development of macrovesicular steatosis, lobular inflammation, and hepatocellular ballooning, all of which were dramatically attenuated by dotinurad (Figure 4C and D). Accordingly, the NAFLD score and serum ALT were significantly higher in HFD-fed mice in comparison with NFD-fed mice, both of which were decreased in dotinurad-treated HFD mice (Figure 4D–F).

Ccl2 and TNFα are proinflammatory M1 macrophage markers and key mediators that lead to hepatic lipogenesis and inflammation in HFD-induced obese mice [11,34]. The hepatic expression of Ccl2 and TNFα was increased in HFD-fed mice in comparison with NFD-fed mice, and dotinurad significantly decreased the levels of these markers (Figure 4G). These results indicate that the URAT1-selective inhibitor treatment significantly improved HFD-induced NAFLD through the inhibition of inflammatory genes.

A recent study showed that high UA induces hepatic steatosis through the NOD-like receptor family pyrin domain containing 3 (NLRP3) inflammasome-dependent mechanism [4], and thus, we next examined NLRP3 in the current model. Although the protein expression of liver NLRP3 in HFD-fed mice was increased in comparison with that in NFD-fed mice, dotinurad did not affect the NLRP3 expression levels (Figure S3A). The difference in the pro-IL1β expression levels of the NFD- and HFD-fed mice was not statistically significant, while dotinurad tended to decrease the level of pro-IL1β in HFD-fed mice (P = 0.08) (Figure S3B). These inconsistent data suggest that URAT1-selective inhibitor treatment may influence the NLRP3 inflammasome-dependent inflammatory pathway in the liver of HFD-fed mice but that its impact is not significant, at least in the present experimental model.

High UA induces the production of intracellular ROS and lipid accumulation in hepatocytes [13]. Thus, we next examined the MDA levels in liver tissues. Liver MDA in HFD-fed mice tended to increase in comparison with NFD-fed mice, while dotinurad decreased it, although these changes were not statistically significant (NFD vs. HFD, P = 0.13; HFD vs. HFD + Doti, P = 0.12) (Figure S3C), indicating that ROS inhibition by URAT1-selective inhibitor treatment may be partly involved in the improvement of HFD-induced NAFLD.

### 3.5. URAT1-selective inhibitor treatment partially promotes the browning of eWAT in HFD-fed mice

WAT could be converted to beige adipose tissue (browning), which possesses the brown-like features of energy dissipation through the activation of the brown adipose-specific protein, UCP1, resulting in the improvement of systemic insulin resistance [15,19]. The previous study showed that the uptake of UA in white adipocytes through URAT1 leads to WAT dysfunction and the impairment of systemic insulin resistance [1]. Thus, we next examined the effects of URAT1-selective inhibitor treatment on eWAT and iWAT. The weight of both eWAT and

 

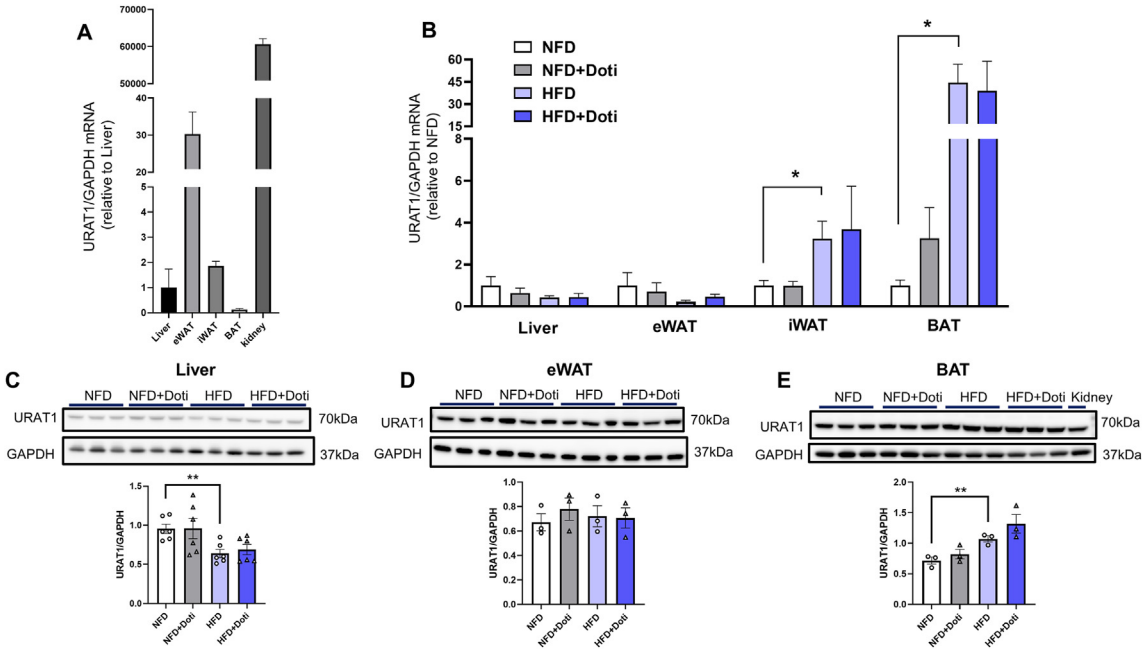


**Figure 3: Relative mRNA profiling and the protein expression of URAT1 in NFD- and HFD-fed mice.** (A) URAT1 mRNA expression in the liver, eWAT, iWAT, BAT, and kidney as assessed by qRT-PCR (n = 3 each). (B) URAT1 mRNA expression in either NFD- or HFD-fed mice with or without dotinurad treatment. ([Liver] n = 6 each; [eWAT] NFD, n = 6; NFD + Doti, n = 6; HFD, n = 6; HFD + Doti, n = 5; [iWAT] NFD, n = 5; NFD + Doti, n = 6; HFD, n = 5; HFD + Doti, n = 5; [BAT] NFD, n = 5; NFD + Doti, n = 4; HFD, n = 6; HFD + Doti, n = 4). The protein expression of URAT1 in liver (C), eWAT (D), and BAT (E) (n = 3 each). Data are expressed as the mean ± SEM. **P < 0.01 and *P < 0.05 between the indicated groups. eWAT, epididymal white adipose tissue; iWAT, inguinal white adipose tissue; BAT, brown adipose tissue.

iWAT were increased in HFD-fed mice in comparison with NFD-fed mice, and dotinurad significantly decreased the weight of eWAT but not iWAT (Figure S4A and B). Although the size of white adipocytes in both eWAT and iWAT was significantly increased by HFD, it was not affected by dotinurad in either adipose tissue under HFD conditions (Figure S4C and D).

We next examined whether URAT1-selective inhibitor treatment induces the browning process in WAT. In iWAT, the UCP1 level tended to

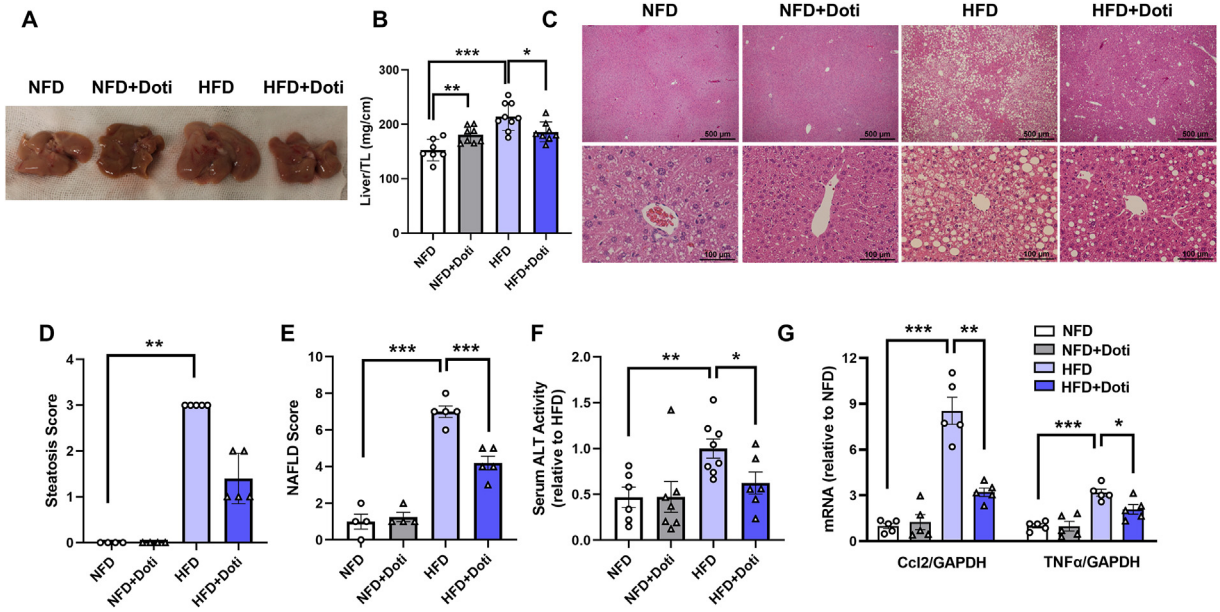


**Figure 4: Effects of URAT1-selective inhibitor treatment on HFD-induced NAFLD.** (A) A representative image of liver harvested from the indicated mice. (B) Liver weight at 4 weeks after treatment with or without dotinurad (NFD, n = 7; NFD + Doti, n = 8; HFD, n = 9; HFD + Doti, n = 8). (C) Hematoxylin and eosin staining of liver sections of mice that received the indicated treatments. (D) Steatosis score (NFD, n = 4; NFD + Doti, n = 4; HFD, n = 5; HFD + Doti, n = 5). (E) NAFLD score (NFD, n = 4; NFD + Doti, n = 4; HFD, n = 5; HFD + Doti, n = 5). (E) Serum ALT activity (NFD, n = 6; NFD + Doti, n = 7; HFD, n = 8; HFD + Doti, n = 6). (F) Relative mRNA expression of Ccl2 and TNFα (n = 5 each). Data are expressed as the mean ± SEM. ***P < 0.001, **P < 0.01, and *P < 0.05 between the indicated groups. NAFLD, nonalcoholic fatty liver disease; TL, tail length.

 

decrease in HFD-fed mice in comparison with NFD-fed mice ($P = 0.07$), which was not affected by dotinurad (Figure S4E). In eWAT, however, the UCP1 level was increased in HFD-fed mice, and dotinurad further increased the UCP1 expression considerably under HFD conditions (Figure S4E). These data indicate that the URAT1-selective inhibitior led to the browning of eWAT in HFD-fed mice, which might partly contribute to the improvement of systemic insulin resistance, as shown in Figure 2.

### 3.6. URAT1-selective inhibitor treatment promotes rebrowning of HFD-induced lipid-rich BAT through UCP1 activation

The BAT weight in HFD-fed mice was significantly increased in comparison with that in NFD-fed mice, and this was reduced by dotinurad (Figure 5A and B). Histological analyses revealed that HFD feeding resulted in so-called BAT 'whitening', which was characterized by increased lipid deposition (Figure 5C). This was markedly attenuated by dotinurad. The lipid droplet size and the diameter of adipocytes in BAT were increased in HFD-fed mice (Figure 5D), and these parameters were significantly decreased by treatment with dotinurad, indicating that URAT1-selective inhibitor treatment might increase lipolysis in BAT. The increased UCP1 expression and UCP1 activity in BAT play an important role in the improvement of glucose tolerance and insulin sensitivity [35]. Thus, we next examined the UCP1 expression in BAT. Histological analyses (Figure 5E) and biochemical analyses of the mRNA (Figure 5F) and protein (Figure 5G) expression revealed that the UCP1 levels in BAT were significantly increased in HFD-fed mice in comparison with those in NFD-fed mice and that they were further increased by treatment with dotinurad. To further evaluate BAT-specific gene expression in BAT, we next examined the mRNA expression of PGC1$\alpha$ and Dio2. The mRNA expression of PGC1$\alpha$ was significantly increased in dotinurad-treated HFD-fed mice in comparison with HFD-fed mice. Dio2 was also increased in dotinurad-treated HFD-fed mice in comparison with HFD-fed mice although the increase was not statistically significant (HFD vs. HFD + Doti, $P = 0.21$) (Figure 5F).

The uptake of UA can increase the oxidative stress in adipocytes, which has recently been recognized as a major cause of insulin resistance [36]. Thus, we measured tissue ROS levels in BAT. The ROS levels in BAT were significantly increased in HFD-fed mice in comparison with NFD-fed mice ([HFD] 450.5 $\pm$ 147 RFU/mg/ml protein vs. [NFD] 112.7 $\pm$ 15.6 RFU/mg/ml protein, $P < 0.05$), which was significantly reduced by treatment with dotinurad ([HFD + Doti] 212.7 $\pm$ 121.3 RFU/mg/ml protein vs. [HFD], $P < 0.05$) (Figure 5H). These results indicate that URAT1-selective inhibitor treatment leads to the '*rebrowning*' of HFD-induced BAT whitening and the reduction of ROS levels in BAT, which contributes to the improvement of systemic insulin resistance.

To determine whether extracellular UA is transported into brown adipocytes through URAT1, we examined the UA uptake in brown adipocytes. The protein expression of URAT1 was detected in the rat brown adipocytes, although its expression was comparable among the groups with the indicated treatments (Figure 5I). When these cells were exposed to a high concentration of UA (15 mg/dl) for either 30 or 60 min, the intracellular UA levels were significantly increased. This was substantially decreased by treatment with dotinurad (Figure 5J). These results demonstrate that URAT1 actually transports UA into the brown adipocytes.

## 4. DISCUSSION

In the present study, we proposed and verified the role and functional significance of URAT1 in metabolic syndrome using a model of diet-induced obesity. We showed that the selective inhibition of URAT1 by dotinurad led to a significant improvement in glucose tolerance and insulin sensitivity in HFD mice. The mechanisms underlying the improvement of insulin resistance by URAT1-selective inhibitor treatment are as follows: (i) URAT1-selective inhibition dramatically improved HFD-induced NAFLD through the inhibition of inflammatory cytokines and (ii) URAT1-selective inhibition led to rebrowning of HFD-induced lipid-rich BAT.

The previous study [9,37] as well as the present study suggested that tissue URAT1 action is enhanced in the insulin-resistant state, as represented by metabolic syndrome, presumably via persistent exposure to hyperinsulinemia. Conversely, the present study indicates that enhanced URAT1 action induces insulin resistance in metabolic syndrome, leading to a vicious cycle (see the Graphical Abstract). In this context, it is possible that URAT1-selective inhibitors are particularly effective in reducing hyperuricemia associated with insulin-resistant metabolic disorders in which the impacts of URAT1 are amplified. In fact, dorinurad treatment ameliorated all indicies of insulin resistance and NAFLD in the current model of metabolic disorders, which might result in the loss of various metabolic organ weights (i.e. eWAT, BAT, and liver), ultimately leading to a slight but significant decrease in body weight.

The development of NAFLD in HFD-induced obese mice is mediated through a complex process driven by multiple factors, such as elevated levels of pro-inflammatory cytokines released from adipose tissues, increased dietary sugars, hypercholesterolemia, and hyperuricemia [38]. In addition, hyperuricemia directly induces fat accumulation and inflammation in hepatocytes through URAT1 *in vitro* [14]. Thus, we assume that dotinurad improves NAFLD through the inhibition of extracellular UA uptake in hepatocytes via URAT1, leading to a reduction in lipid deposition and inflammation. Another possibility is that rebrowning of BAT and browning of eWAT may indirectly ameliorate NAFLD via adipokines and batokines, such as adiponectin, neuregulin 4, and fibroblast growth factor 21, all of which have been reported to improve steatosis [15].

Serum NEFA levels are elevated generally as a consequence of enhanced lipolysis in HFD-fed mice. However, we found that serum free fatty acid levels were comparable between NFD- and HFD-fed mice, and dotinurad treatment did not significantly affect them, which was consistent with the finding of our previous study [18]. This might be because the blood samples were collected after a substantial period of fasting, which resulted in the stimulation of lipolysis in adipose tissues even in the NFD-fed mice [39].

UA is also taken up into the adipocytes via URAT1 and induces both ROS synthesis and inflammation, leading to the impairment of systemic insulin resistance [1]. Meanwhile, it has been shown that ROS inhibition leads to UCP1 activation and *vice versa* in brown adipocytes [40]. The present *in vitro* study confirmed the extracellular uptake of UA into brown adipocytes via URAT1 (Figure 5J). Moreover, we found that HFD feeding increased the URAT1 expression in BAT (Figure 3B and E), which is consistent with the previously reported findings in the kidney [9], and that HFD feeding induced ROS synthesis in BAT, which was substantially reduced by treatment with dotinurad (Figure 5H). Taking these findings together, we assume that the enhanced uptake of UA into the brown adipocytes through URAT1 in the HFD-fed mice induced tissue ROS synthesis, resulting in BAT whitening. Thus, the inhibition of the upregulated URAT1 in the BAT of HFD-fed mice reduces the intracellular UA and ROS levels, leading to the upregulation of UCP1. To the best of our knowledge, this is the first study to report that the inhibition of the upregulated URAT1 in HFD-fed mice plays a substantial role in the rebrowning of lipid-rich BAT.

 

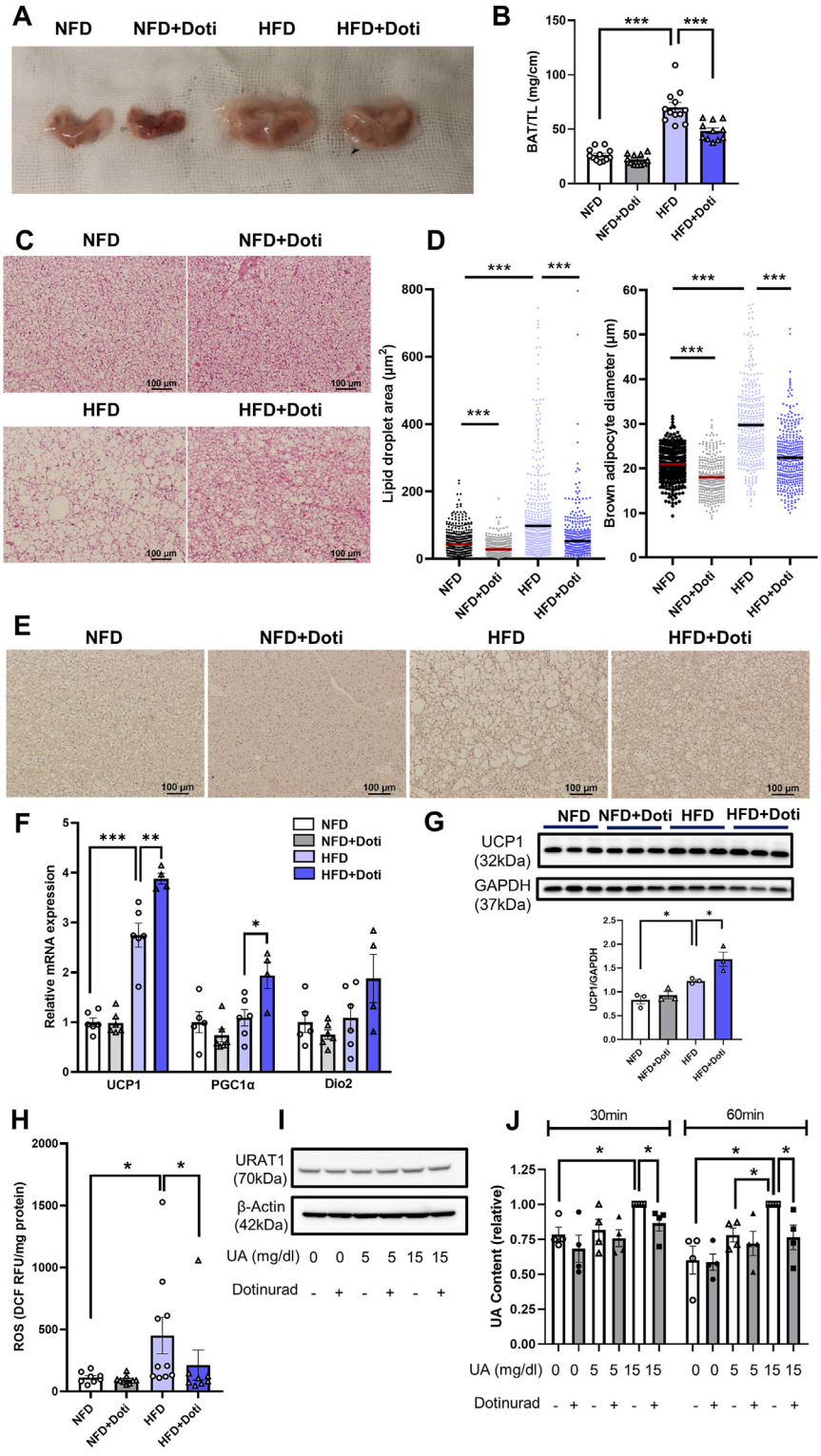


**Figure 5: Effects of URAT1-selective inhibitor treatment on HFD-induced lipid-rich BAT.** (A) A representative image of BAT harvested from the indicated mice. (B) BAT weight (NFD, n = 12; NFD + Doti, n = 11; HFD, n = 12; HFD + Doti, n = 11). (C) Hematoxylin and eosin staining of the BAT section of mice with the indicated treatments. (D) Lipid droplet area and brown adipocyte diameter were measured in the indicated mice (n = 3 each) ([Lipid droplet area] NFD, n = 607; NFD + Doti, n = 609; HFD, n = 624; HFD + Doti, n = 610; [Brown adipocyte diameter] NFD, n = 297; NFD + Doti, n = 305; HFD, n = 335; HFD + Doti, n = 353). (E) UCP1 immunostaining in BAT. (F) Relative mRNA expressions of UCP1, PGC1α, and Dio2 ([UCP1] NFD, n = 6; NFD + Doti, n = 6; HFD, n = 6; HFD + Doti, n = 4; [PGC1α and Dio2] NFD, n = 5; NFD + Doti, n = 6; HFD, n = 6; HFD + Doti, n = 4). (G) The protein expression of UCP1 (n = 3 each). (H) Total ROS was measured by determining the fluorescence of DCF (DCF RFU: Dichlorofluorescein Relative Fluorescence Units) (NFD, n = 8; NFD + Doti, n = 9; HFD, n = 10; HFD + Doti, n = 8). (I) The URAT1 expression in primary brown adipocytes exposed to the indicated treatments for 24 h. (J) The intracellular UA levels in primary brown adipocytes exposed to the indicated treatments for 30 min and 60 min (n = 4 each). Data are expressed as the mean ± SEM. ***P < 0.001, **P < 0.01, and *P < 0.05 between the indicated groups. UA, uric acid; ROS, reactive oxygen species.

 

Regarding WAT, we found that the responses of UCP1 to dotinurad differed between iWAT and eWAT (Figure S4E). This might be due to the differences in the URAT1 expression between these WATs; namely, the URAT1 expression was substantially higher in eWAT than in iWAT, as shown in Figure 3A. Therefore, dotinurad may have a more marked impact on eWAT than on iWAT. A previous study showed that the enhanced UA uptake into WAT via URAT1 and the subsequent increase in the intracellular UA levels led to the inhibition of the leptin-AMPK pathway, which resulted in a reduction in the UCP1 expression in WAT [19]. These results, along with the fact that the URAT1 expression was higher in eWAT than in iWAT, support the present findings that dotinurad increased the UCP1 expression only in the eWAT of HFD-fed mice, not in iWAT. However, further investigations are required to elucidate the precise mechanisms by which intracellular UA regulates the UCP1 expression in WAT.

On the other hand, HFD alone also increased the UCP1 expression in both eWAT and BAT, consistent with previous studies [18,41], presumably as an adaptive mechanism for fatty acid overload [15,18]. However its pathophysiological significance in the present study model remains unclear.

The previous *in vivo* studies and clinical trials showed that nonselective URAT1 inhibitors, such as benzbromarone, also improve systemic insulin resistance [1,19,42]. However, benzbromarone non-specifically interferes with some urate secretion transporters, such as ATP-binding cassette subfamily G membrane 2 (ABCG2), organic anion transporter 1 (OAT1), and OAT3 [20], which make it unfavorable as a UA-lowering agent. In addition, several reports have shown that benzbromarone causes hepatotoxicity through apoptosis and ROS synthesis, especially in HFD-induced obese mice [43,44]. Therefore, the present study underscores the clinical significance of dotinurad for the treatment of metabolic disorders, since this novel agent more selectively inhibits URAT1 [23].

In general, hyperuricemia is classified into three categories depending on the mechanisms [45]: the urate overproduction type, the underexcretion type, and the combined type. In the present study, although the UA levels tended to be lower in dotinurad-treated HFD-fed mice than in HFD-fed mice without dotinurad treatment, the difference failed to reach statistical significance (Table 1). Previous studies indicate that the URAT1 function in mice kidney is not as high as that in humans as described previously [20,46]; therefore, dotinurad would have a less significant impact on plasma UA levels per se. This is because in most mammals other than humans, UA is easily metabolized to allantoin by uricase. Consequently, much less UA is reabsorbed in the kidneys [20,47]. It is also possible that dotinurad affects the tissue distribution of UA. We found in the present study that URAT1 was substantially expressed in various tissues, including eWAT, iWAT, BAT, and liver (Figure 3B—E), other than in the kidneys, where URAT1 is primarily present. Therefore, dotinurad might inhibit the uptake of extracellular UA into those tissues and cells (as shown in Figure 5J), resulting in a relatively small change in plasma UA levels. Therefore, the mechanism of hyperuricemia in the current HFD mice might be largely due to the overproduction of urate, mainly in the liver [48]. As such, the decreased hepatic URAT1 expression observed in the HFD mice might be a compensatory reaction to the overproduction of UA in the hepatocytes, resulting from the activation of the xanthine oxidoreductase and polyol pathways observed in the models of diet-induced obesity [11,48].

The reason why dotinurad increased liver weight in NFD mice remains elusive. Given that dotinurad affected neither all the indices of NAFLD activity (i.e. steatosis score, NAFLD score, and serum ALT activity) nor the inflammatory markers (i.e. hepatic inflammatory citokines and MDA content) in NFD, it might be due to a non-adverse adaptive response to dotinurad administered in pharmacological doses [49]. In the present study, we used a pharmacological dose of dotinurad because of its low sensitivity toward murine URAT1 in the kidneys.

The present study suffers from some limitations. First, since UA is easily metabolized by uricase and is much less reabsorbed in the kidneys in rodents, as already discussed, the metabolomics of UA in mice might differ from that in humans. Second, as URAT1 is also expressed in macrophages [50] and vascular smooth muscle cells [51], further investigations on the precise location at which URAT1 is expressed in the liver tissue are warranted to fully clarify the pathophysiological role of URAT1 in NAFLD. Third, since a relatively high dose of dotinurad is used, it would be difficult to exclude that some of the effects are caused by off-target effects. Further studies are warranted to fully determine the pathophysiological role of URAT1 using *in vitro* and *in vivo* models of genetic URAT1 knockdown.

## 5. CONCLUSIONS

URAT1-selective inhibitor treatment ameliorates systemic insulin resistance in diet-induced obese mice. URAT1-selective inhibitor treatment functionally and histologically improves NAFLD through the inhibition of Ccl2 and TNF$\alpha$. Furthermore, the increased URAT1 expression levels in the BAT of HFD-fed mice induce BAT whitening and tissue ROS synthesis, and URAT1-selective inhibitor treatment leads to rebrowning of HFD-induced lipid-rich BAT, resulting in the reduction of ROS. Taking the results together, the present study reports that pharmacological URAT1-selective inhibition has therapeutic potential for hyperuricemia, which is associated with various insulin-resistant metabolic disorders, including NAFLD.

## FUNDING

This work was supported in part by grants-in-aid from the Ministry of Education Culture, Sports, Science and Technology (JP20K08435 to T.N., JP21K16099 to H. K., and JP19K08592 to M.Y.) and SENSHIN Medical Research Foundation to T.N.

## AUTHOR CONTRIBUTIONS

Y. Tanaka, T. Nagoshi, and M. Yoshimura conceived and designed the study and contributed to the writing of the manuscript; Y. Tanaka, A. Yoshii, Y. Oi, H. Takahashi, and H. Kimura conducted the experiments and contributed to the acquisition and interpretation of the data; K. Ito, Y. Kashiwagi, and T. D. Tanaka analyzed and interpreted the data and critically revised the manuscript. All authors read and approved the final manuscript.

## ACKNOWLEDGMENTS

The authors are grateful to Prof. Masahiro Ikegami (Department of Pathology, The Jikei University School of Medicine) for his excellent technical support.

## CONFLICT OF INTEREST

No potential conflicts of interest relevant to this article were reported. Outside this study, M.Y. reports lecture fees from Mochida Pharmaceutical Co., Ltd., Fujiyakuhin Co., Ltd., Daiichi Sankyo Co., Ltd., Pfizer Japan Inc., and Kowa Co., Ltd.; grants and lecture fees from Mitsubishi Tanabe Pharma Corporation; and grants from Teijin Pharma Ltd., Astellas Pharma Inc., and Shionogi & Co., Ltd.

 

## APPENDIX A. SUPPLEMENTARY DATA

Supplementary data to this article can be found online at https://doi.org/10.1016/j.molmet.2021.101411.

## REFERENCES


[1] Baldwin, W., McRae, S., Marek, G., Wymer, D., Pannu, V., Baylis, C., et al., 2011. Hyperuricemia as a mediator of the proinflammatory endocrine imbalance in the adipose tissue in a murine model of the metabolic syndrome. Diabetes 60(4):1258—1269.

[2] Tanaka, Y., Nagoshi, T., Kawai, M., Uno, G., Ito, S., Yoshii, A., et al., 2017. Close linkage between serum uric acid and cardiac dysfunction in patients with ischemic heart disease according to covariance structure analysis. Scientific Reports 7(1):2519.

[3] Tanaka, Y., Nagoshi, T., Yoshii, A., Oi, Y., Takahashi, H., Kimura, H., et al., 2021. Xanthine oxidase inhibition attenuates doxorubicin-induced cardiotoxicity in mice. Free Radical Biology and Medicine 162:298—308.

[4] Wan, X., Xu, C., Lin, Y., Lu, C., Li, D., Sang, J., et al., 2016. Uric acid regulates hepatic steatosis and insulin resistance through the NLRP3 inflammasome-dependent mechanism. Journal of Hepatology 64(4):925—932.

[5] Harmon, D.B., Mandler, W.K., Sipula, I.J., Dedousis, N., Lewis, S.E., Eckels, J.T., et al., 2019. Hepatocyte-specific ablation or whole-body inhibition of xanthine oxidoreductase in mice corrects obesity-induced systemic hyperuricemia without improving metabolic abnormalities. Diabetes 68(6):1221—1229.

[6] Zhi, L., Yuzhang, Z., Tianliang, H., Hisatome, I., Yamamoto, T., Jidong, C., 2016. High uric acid induces insulin resistance in cardiomyocytes in vitro and in vivo. PLoS One 11(2):e0147737.

[7] Enomoto, A., Kimura, H., Chairoungdua, A., Shigeta, Y., Jutabha, P., Cha, S.H., et al., 2002. Molecular identification of a renal urate anion exchanger that regulates blood urate levels. Nature 417(6887):447—452.

[8] Sugihara, S., Hisatome, I., Kuwabara, M., Niwa, K., Maharani, N., Kato, M., et al., 2015. Depletion of uric acid due to SLC22A12 (URAT1) loss-of-function mutation causes endothelial dysfunction in hypouricemia. Circulation Journal 79(5):1125—1132.

[9] Toyoki, D., Shibata, S., Kuribayashi-Okuma, E., Xu, N., Ishizawa, K., Hosoyamada, M., et al., 2017. Insulin stimulates uric acid reabsorption via regulating urate transporter 1 and ATP-binding cassette subfamily G member 2. American Journal of Physiology. Renal Physiology 313(3):F826—F834.

[10] Ogino, K., Kato, M., Furuse, Y., Kinugasa, Y., Ishida, K., Osaki, S., et al., 2010. Uric acid-lowering treatment with benzbromarone in patients with heart failure: a double-blind placebo-controlled crossover preliminary study. Circulation. Heart Failure 3(1):73—81.

[11] Nishikawa, T., Nagata, N., Shimakami, T., Shirakura, T., Matsui, C., Ni, Y., et al., 2020. Xanthine oxidase inhibition attenuates insulin resistance and diet-induced steatohepatitis in mice. Scientific Reports 10(1):815.

[12] Savari, F., Mard, S.A., Badavi, M., Rezaie, A., Gharib-Naseri, M.K., 2019. A new method to induce nonalcoholic steatohepatitis (NASH) in mice. BMC Gastroenterology 19(1):125.

[13] Sanchez-Lozada, L.G., Andres-Hernando, A., Garcia-Arroyo, F.E., Cicerchi, C., Li, N., Kuwabara, M., et al., 2019. Uric acid activates aldose reductase and the polyol pathway for endogenous fructose and fat production causing development of fatty liver in rats. Journal of Biological Chemistry 294(11):4272—4281.

[14] Spiga, R., Marini, M.A., Mancuso, E., Di Fatta, C., Fuoco, A., Perticone, F., et al., 2017. Uric acid is associated with inflammatory biomarkers and induces inflammation via activating the NF-κB signaling pathway in HepG2 cells. Arteriosclerosis, Thrombosis, and Vascular Biology 37(6):1241—1249.

[15] Czech, M.P., 2020. Mechanisms of insulin resistance related to white, beige, and brown adipocytes. Molecular Metabolism 34:27—42.

[16] Kimura, H., Nagoshi, T., Yoshii, A., Kashiwagi, Y., Tanaka, Y., Ito, K., et al., 2017. The thermogenic actions of natriuretic peptide in brown adipocytes: the direct measurement of the intracellular temperature using a fluorescent thermoprobe. Scientific Reports 7(1):12978.

[17] Shimizu, I., Aprahamian, T., Kikuchi, R., Shimizu, A., Papanicolaou, K.N., MacLauchlan, S., et al., 2014. Vascular rarefaction mediates whitening of brown fat in obesity. Journal of Clinical Investigation 124(5):2099—2112.

[18] Kimura, H., Nagoshi, T., Oi, Y., Yoshii, A., Tanaka, Y., Takahashi, H., et al., 2021. Treatment with atrial natriuretic peptide induces adipose tissue browning and exerts thermogenic actions in vivo. Scientific Reports 11(1):17466.

[19] Su, M., Sun, L., Li, W., Liu, H., Liu, Y., Wei, Y., et al., 2020. Metformin alleviates hyperuricaemia-induced serum FFA elevation and insulin resistance by inhibiting adipocyte hypertrophy and reversing suppressed white adipose tissue beiging. Clinical Science 134(12):1537—1553.

[20] Taniguchi, T., Ashizawa, N., Matsumoto, K., Saito, R., Motoki, K., Sakai, M., et al., 2019. Pharmacological evaluation of dotinurad, a selective urate reabsorption inhibitor. The Journal of Pharmacology and Experimental Therapeutics 371(1):162—170.

[21] Tan, P.K., Liu, S., Gunic, E., Miner, J.N., 2017. Discovery and characterization of verinurad, a potent and specific inhibitor of URAT1 for the treatment of hyperuricemia and gout. Scientific Reports 7(1):665.

[22] Miner, J.N., Tan, P.K., Hyndman, D., Liu, S., Iverson, C., Nanavati, P., et al., 2016. Lesinurad, a novel, oral compound for gout, acts to decrease serum uric acid through inhibition of urate transporters in the kidney. Arthritis Research and Therapy 18(1):214.

[23] Hosoya, T., Sano, T., Sasaki, T., Fushimi, M., Ohashi, T., 2020. Clinical efficacy and safety of dotinurad, a novel selective urate reabsorption inhibitor, in Japanese hyperuricemic patients with or without gout: randomized, multicenter, double-blind, placebo-controlled, parallel-group, confirmatory phase 2 study. Clinical and Experimental Nephrology 24(Suppl 1):53—61.

[24] Yoshii, A., Nagoshi, T., Kashiwagi, Y., Kimura, H., Tanaka, Y., Oi, Y., et al., 2019. Cardiac ischemia-reperfusion injury under insulin-resistant conditions: SGLT1 but not SGLT2 plays a compensatory protective role in diet-induced obesity. Cardiovascular Diabetology 18(1):85.

[25] Lee, E.S., Kwon, M.H., Kim, H.M., Woo, H.B., Ahn, C.M., Chung, C.H., 2020. Curcumin analog CUR5-8 ameliorates nonalcoholic fatty liver disease in mice with high-fat diet-induced obesity. Metabolism 103:154015.

[26] Le Duc, D., Lin, C.-C., Popkova, Y., Yang, Z., Akhil, V., Çakir, M.V., et al., 2020. Reduced lipolysis in lipoma phenocopies lipid accumulation in obesity. International Journal of Obesity 45(3):565—576.

[27] Sun, W., Uchida, K., Suzuki, Y., Zhou, Y., Kim, M., Takayama, Y., et al., 2016. Lack of TRPV2 impairs thermogenesis in mouse brown adipose tissue. EMBO Reports 17(3):383—399.

[28] Matthaeus, C., Lahmann, I., Kunz, S., Jonas, W., Melo, A.A., Lehmann, M., et al., 2020. EHD2-mediated restriction of caveolar dynamics regulates cellular fatty acid uptake. Proceedings of the National Academy of Sciences of the United States of America 117(13):7471—7481.

[29] Shimizu, N., Maruyama, T., Yoshikawa, N., Matsumiya, R., Ma, Y., Ito, N., et al., 2015. A muscle-liver-fat signalling axis is essential for central control of adaptive adipose remodelling. Nature Communications 6(1):6693.

[30] Lim, P.J., Duarte, T.L., Arezes, J., Garcia-Santos, D., Hamdi, A., Pasricha, S.R., et al., 2019. Nrf2 controls iron homeostasis in haemochromatosis and thalassaemia via Bmp6 and hepcidin. Nature Metabolism 1(5):519—531.

[31] Alcala, M., Calderon-Dominguez, M., Bustos, E., Ramos, P., Casals, N., Serra, D., et al., 2017. Increased inflammation, oxidative stress and mitochondrial respiration in brown adipose tissue from obese mice. Scientific Reports 7(1):16082.

[32] Shen, H., Jiang, L., Lin, J.D., Omary, M.B., Rui, L., 2019. Brown fat activation mitigates alcohol-induced liver steatosis and injury in mice. Journal of Clinical Investigation 129(6):2305—2317.


 

[33] Kanellis, J., Watanabe, S., Li, J.H., Kang, D.H., Li, P., Nakagawa, T., et al., 2003. Uric acid stimulates monocyte chemoattractant protein-1 production in vascular smooth muscle cells via mitogen-activated protein kinase and cyclooxygenase-2. Hypertension 41(6):1287—1293.

[34] Liu, W., Struik, D., Nies, V.J.M., Jurdzinski, A., Harkema, L., de Bruin, A., et al., 2016. Effective treatment of steatosis and steatohepatitis by fibroblast growth factor 1 in mouse models of nonalcoholic fatty liver disease. Proceedings of the National Academy of Sciences of the United States of America 113(8):2288.

[35] Kwon, M.M., O'Dwyer, S.M., Baker, R.K., Covey, S.D., Kieffer, T.J., 2015. FGF21-mediated improvements in glucose clearance require uncoupling protein 1. Cell Reports 13(8):1521—1527.

[36] Sautin, Y.Y., Nakagawa, T., Zharikov, S., Johnson, R.J., 2007. Adverse effects of the classic antioxidant uric acid in adipocytes: NADPH oxidase-mediated oxidative/nitrosative stress. American Journal of Physiology - Cell Physiology 293(2):C584—C596.

[37] Matsubayashi, M., Sakaguchi, Y.M., Sahara, Y., Nanaura, H., Kikuchi, S., Asghari, A., et al., 2021. 27-Hydroxycholesterol regulates human SLC22A12 gene expression through estrogen receptor action. FASEB Journal 35(1): e21262.

[38] Friedman, S.L., Neuschwander-Tetri, B.A., Rinella, M., Sanyal, A.J., 2018. Mechanisms of NAFLD development and therapeutic strategies. Nature Medicine 24(7):908—922.

[39] Karpe, F., Dickmann, J.R., Frayn, K.N., 2011. Fatty acids, obesity, and insulin resistance: time for a reevaluation. Diabetes 60(10):2441—2449.

[40] Cui, X., Xiao, W., You, L., Zhang, F., Cao, X., Feng, J., et al., 2019. Age-induced oxidative stress impairs adipogenesis and thermogenesis in brown fat. FEBS Journal 286(14):2753—2768.

[41] Ishii, A., Katsuura, G., Imamaki, H., Kimura, H., Mori, K.P., Kuwabara, T., et al., 2017. Obesity-promoting and anti-thermogenic effects of neutrophil gelatinase-associated lipocalin in mice. Scientific Reports 7(1):15501.

[42] Cai, H.-y., Wang, T., Zhao, J.-c., Sun, P., Yan, G.-r., Ding, H.-p., et al., 2013. Benzbromarone, an old uricosuric drug, inhibits human fatty acid binding protein 4 in vitro and lowers the blood glucose level in db/db mice. Acta Pharmacologica Sinica 34(11):1397—1402.

[43] Sun, P., Zhu, J.J., Wang, T., Huang, Q., Zhou, Y.R., Yu, B.W., et al., 2018. Benzbromarone aggravates hepatic steatosis in obese individuals. Biochimica et Biophysica Acta - Molecular Basis of Disease 1864(6 Pt A):2067—2077.

[44] Kaufmann, P., Torok, M., Hanni, A., Roberts, P., Gasser, R., Krahenbuhl, S., 2005. Mechanisms of benzarone and benzbromarone-induced hepatic toxicity. Hepatology 41(4):925—935.

[45] Ichida, K., Matsuo, H., Takada, T., Nakayama, A., Murakami, K., Shimizu, T., et al., 2012. Decreased extra-renal urate excretion is a common cause of hyperuricemia. Nature Communications 3:764.

[46] Novikov, A., Fu, Y., Huang, W., Freeman, B., Patel, R., van Ginkel, C., et al., 2019. SGLT2 inhibition and renal urate excretion: role of luminal glucose, GLUT9, and URAT1. American Journal of Physiology. Renal Physiology 316(1): F173—F185.

[47] Preitner, F., Pimentel, A., Metref, S., Berthonneche, C., Sarre, A., Moret, C., et al., 2015. No development of hypertension in the hyperuricemic liver-Glut9 knockout mouse. Kidney International 87(5):940—947.

[48] Johnson, R.J., Nakagawa, T., Sanchez-Lozada, L.G., Shafiu, M., Sundaram, S., Le, M., et al., 2013. Sugar, uric acid, and the etiology of diabetes and obesity. Diabetes 62(10):3307—3315.

[49] Hall, A.P., Elcombe, C.R., Foster, J.R., Harada, T., Kaufmann, W., Knippel, A., et al., 2012. Liver hypertrophy: a review of adaptive (adverse and non-adverse) changes–conclusions from the 3rd International ESTP Expert Workshop. Toxicologic Pathology 40(7):971—994.

[50] Martínez-Reyes, C.P., Manjarrez-Reyna, A.N., Méndez-García, L.A., Aguayo-Guerrero, J.A., Aguirre-Sierra, B., Villalobos-Molina, R., et al., 2020. Uric acid has direct proinflammatory effects on human macrophages by increasing proinflammatory mediators and bacterial phagocytosis probably via URAT1. Biomolecules 10(4).

[51] Price, K.L., Sautin, Y.Y., Long, D.A., Zhang, L., Miyazaki, H., Mu, W., et al., 2006. Human vascular smooth muscle cells express a urate transporter. Journal of the American Society of Nephrology 17(7):1791—1795.

 